Regenerative Therapy 22 (2023) 210–223

Contents lists available at ScienceDirect

Regenerative Therapy

journal homepage: http://www.elsevier.com/locate/reth

Original Article

Therapeutic role of adipose-derived mesenchymal stem cells-derived extracellular vesicles in rats with obstructive sleep apnea hypopnea syndrome

Lin Xu [a, b], Lu Zhang [b], Yang Xiang [c], Xiangyan Zhang [b, *]

[a] Guizhou University Medical College, Guiyang City, 550025, Guizhou Province, 550025, China
[b] Pulmonary and Critical Care Medicine, Guizhou Provincial People's Hospital, Guiyang City, Guizhou Province, 550002, China
[c] Department of Oncology, Guizhou Provincial People's Hospital, Guiyang City, Guizhou Province, 550002, China

ARTICLE INFO

Article history:
Received 5 December 2022
Received in revised form
3 January 2023
Accepted 12 January 2023

Keywords:
Obstructive sleep apnea hypopnea syndrome
Lung injury
Adipose-derived mesenchymal stem cells
Extracellular vesicles
miR-22–3p

ABSTRACT

Background: Obstructive sleep apnea hypopnea syndrome (OSAHS) is an underestimated sleep disorder that leads to multiple organ damages, including lung injury (LI). This paper sought to analyze the molecular mechanism of extracellular vesicles (EVs) from adipose-derived mesenchymal stem cells (ADSCs) in OSAHS-induced lung injury (LI) via the miR-22–3p/histone lysine demethylase 6 B (KDM6B)/high mobility group AT-hook 2 (HMGA2) axis.

Methods: ADSCs and ADSCs-EVs were separated and characterized. Chronic intermittent hypoxia (CIH) was used to mimic OSAHS-LI, followed by ADSCs-EVs treatment and hematoxylin and eosin staining, TUNEL, ELISA, and assays of inflammation and oxidative stress (MPO/ROS/MDA/SOD). The CIH cell model was established and treated with ADSCs-EVs. Cell injury was assessed by the assays of MTT, TUNEL, ELISA, and others. Levels of miR-22–3p, KDM6B, histone H3 trimethylation at lysine 27 (H3K27me3), and HMGA2 were determine by RT-qPCR or Western blot analysis. The transfer of miR-22–3p by ADSCs-EVs was observed by fluorescence microscopy. Gene interactions were analyzed by dual-luciferase assay or chromatin immunoprecipitation.

Results: ADSCs-EVs effectively alleviated OSAHS-LI by reducing lung tissue injury, apoptosis, oxidative stress, and inflammation. *In vitro*, ADSCs-EVs increased cell viability and reduced apoptosis, inflammation and oxidative stress. ADSCs-EVs delivered enveloped miR-22–3p into pneumonocytes to upregulate miR-22–3p expression, inhibit KDM6B expression, increase H3K27me3 levels on the HMGA2 promoter, and decrease HMGA2 mRNA levels. Overexpression of KDM6B or HMGA2 attenuated the protective role of ADSCs-EVs in OSAHS-LI.

Conclusion: ADSCs-EVs transferred miR-22–3p to pneumonocytes and reduced apoptosis, inflammation, and oxidative stress through KDM6B/HMGA2, mitigating OSAHS-LI progression.

1. Introduction

Obstructive sleep apnea hypopnea syndrome (OSAHS) is an underdiagnosed disease defined by partial or complete recurrent pauses in ventilation, affecting 2%–5% of the middle-aged population [1]. It is associated with both nocturnal and diurnal symptoms, including snoring, fragmented sleep, asthenia, hallucination, and depression [2]. Chronic intermittent hypoxia (CIH), characterized by episodes of apnea and hypopnea, is regarded as the major cause of oxidative stress (OS) and inflammation, contributing to OSAHS-associated complications [3,4]. As a result, the CIH animal model is commonly established by controlling the ambient oxygen concentration to mimic human OSAHS condition due to the similarity on hypoxia property. In addition, CIH can result in pathological changes in the lung, such as inflammatory infiltration, fibrosis, and OS [5]. Hence, it is significant to analyze the molecular indexes involved in OSAHS and CIH conditions to

* Corresponding author. Pulmonary and Critical Care Medicine, Guizhou Provincial People's Hospital, No. 83, Zhongshan East Road, Nanming District, Guiyang City, Guizhou Province, 550002, China.
E-mail address: zzhangxiangyan@163.com (X. Zhang).

Peer review under responsibility of the Japanese Society for Regenerative Medicine.

https://doi.org/10.1016/j.reth.2023.01.003

provide novel insights into the diagnosis and treatment of OSAHS-induced lung injury (LI).

Mesenchymal stem cells (MSCs) are a class of pluripotent stem cells derived from multiple tissues types, including bone marrow, adipose, umbilical cord, and others, with extraordinary abilities of self-renew, migration, and differentiation [6]. Adipose-derived mesenchymal stem cells (ADSCs) are nominated as a promising therapy for tissue repair due to its secretory function [7]. ADSCs can secrete lipid bilayer-bound exosomes (40–200 nm diameter), also known as extracellular vesicles (EVs) that play a role in cell proliferation, apoptosis, angiogenesis, metabolism, and inflammation, thus exerting therapeutic functions in various human diseases, including pulmonary diseases [8]. In particular, ADSCs-EVs are endowed with anti-apoptotic, anti-inflammatory, and anti-oxidative stress properties to alleviate hyperoxia-induced lung injury [9]. However, compared with the detailed study of bone marrow-derived MSCs (BMSCs), the role of ADSCs and its secreted EVs in OSAHS-LI remains elusive.

On another note, ADSCs-EVs has been identified as a potential therapeutic approach based on the delivery of proteins or RNAs, such as microRNAs (miRNAs), and immunomodulatory properties [10]. miRNAs are established as highly conserved small transcripts with an ability to promote the degradation of messenger RNAs (mRNAs) and are crucial for lung development and diseases [11,12]. A prior study has demonstrated that miR-22–3p functions as an exosome secreted by human umbilical cord blood-derived MSCs to play a protective role against lipopolysaccharide (LPS)-induced acute lung injury [13]. Besides, it has been uncovered as a down-regulated circulating miRNA in patients with OSAHS [14]. Furthermore, our bioinformatics revealed lysine-specific demethylase 6 B (KDM6B/JMJD3) as a downstream target gene of miR-22–3p, suggesting the regulatory role of miR-22–3p in KDM6B expression. KDM6B overexpression has been unveiled to exacerbate ischemia/reperfusion-induced lung injury which is similar to the CIH condition [15]. What's more, KDM6B is preferentially recruited to the gene promoter characteristic of high modification of trimethylated H3K27 (H3K4me3), leading to H3K4me3 inhibition and gene activation [16]. High mobility group AT-hook 2 (HMGA2) has been shown to fuel the pathogenesis of pulmonary fibrosis [17,18]. Besides, there is H3K27me3 modification on the HMGA2 promoter [19], hinting at the association between HMGA2 and KDM6B-meidated demethylation of H3K27.

Given the currently available evidences, we hypothesized that ADSCs-EVs mediate the transport of miR-22–3p to regulate the KDM6B/HMGA2 axis and play a therapeutic role in OSAHS-LI. Consequently, our study aimed to expound on the molecular mechanism of ADSCs-EVs in OSAHS-LI and provide a novel rationale for the disease treatment.

2. Materials and methods

2.1. Experimental animals

Male Sprague Dawley's (SD) rats (about 8 weeks, 180–230 g) were procured from Zhejiang Vital River Laboratory Animal Technology Co., Ltd (SYXK (Zhejiang), 2019–0003) and housed in the setting conditions (12/12 h light/dark cycles, 60% ± 5% humidity, and 22 ± 3 °C temperature) with ad libitum access to fodder and water. All animal experiments were conducted following the guidelines ratified by the Ethics Committee of Guizhou Provincial People's Hospital. After the finishing of experiments, all mice were euthanatized. Extensive methods were undertaken to reduce the animal number and pain as much as possible.

2.2. Preparation, culture, and characterization of ADSCs

The separation and culture of ADSCs were conducted according to a previous method [20]. Briefly, adipose tissues were extracted from the groin of SD rats and washed with phosphate buffer saline (PBS) to remove the residual blood. Then, tissues were sliced into 1 × 1 mm^3 pieces and were detached with collagenase I. Upon 5 min centrifugation at 4000*g*, cell particles were preserved in Dulbecco's modified Eagle medium (DMEM) incorporated with 10% fetal bovine serum (FBS)/1% penicillin-streptomycin/2 mM L-Glutamine and were cultured under a humidified environment of 5% CO_2 and 37 °C for 48 h. Subsequently, the culture medium containing non-adherent cells were removed, followed by the addition of fresh medium. The medium was replaced every 3 days. Cells underwent passage upon reaching 90% confluence. The third generation of ADSCs were used for the subsequent experiments.

The surface markers (CD105, CD34, CD44, and CD45) of ADSCs were identified with a flow cytometer (BD Biosciences, San Jose, CA, USA). Simply put, ADSCs were incubated with antibodies against CD105 (MA1-19594), CD34 (PA5-85917), CD44 (MA5-17522), and CD45 (11-0461-82) at 4 °C for 1 h. Antibodies were purchased from Thermo Fisher Scientific (Waltham, MA, USA).

The assays about adipogenesis and osteogenic differentiation were conducted. In terms of osteogenic differentiation, ADSCs were cultured in osteogenic induction medium comprised of DMDM containing 10% FBS, ascorbic acid, β-glycerophosphate, and dexamethasone, aiming to induce osteogenic differentiation. In terms of adipogenesis, ADSCs were cultured in adipogenic induction medium comprised of DMEM containing 10% FBS, insulin, indomethacin, dexamethasone, and 3-isobutyl-1-methylxanthine. The medium was replaced every 3–4 days for a duration of 21 days. Then, cells were fixed and stained with alizarin red and oil red O staining. The reagents were all purchased from Solarbio (Beijing, China).

2.3. Treatment of ADSCs

With the application of Lipofectamine 3000 (Invitrogen, Carlsbad, CA, USA), miR-22–3p mimic (mimic) and its negative control were transfected into ADSCs. After 48 h, EVs were separated. In addition, ADSCs were treated with RNase A (Sigma, 2 mg/mL) or 0.1% Triton X-100 to identify whether miR-22–3p exists in the membrane structure.

2.4. Separation and characterization of EVs in the conditioned medium

Upon reaching 80–90% confluence, ADSCs were rinsed with PBS and cultured in the culture medium. Then, ADSCs were centrifuged at 300 g for 10 min, followed by another round of 10 min centrifugation at 2000*g* to remove died cells and cell debris. After 30 min centrifugation at 10000*g*, the supernatant was filtered with a 0.22 μm filter (Millipore, Bedford, MA, USA). Next, 15 mL supernatant was transferred into Amicon Ultra-15 Centrifugal Filter Unit (100 kDa, Millipore) and concentrated to 1 mL by 4000 g centrifugation. The ultrafiltration unit was washed with PBS twice and the recycled samples were re-centrifuged at 4000 g to reach 1 mL volume. A 1/5 volume of ExoQuick exosome precipitation solution (System Biosciences, Palo Alto, CA, USA) was added to the ultrafiltrate and mixed upside down to homogenize. After 12 h incubation, the mixture was treated with 30 min centrifugation at 1500*g* and the supernatant was discarded. Subsequently, EVs particles were resuspended with 500 μL PBS. All operations were carried out at

4 °C. The representative makers of EVs CD9 (1:500, MA5-31980, Thermo Fisher Scientific), CD63 (1:500, PA5-92370, Thermo Fisher Scientific), and Calnexin (1:5000, PA5-34754, Thermo Fisher Scientific) were determined through Western blot assay. The morphology and particle diameter of EVs were observed with a transmission electron microscope (TEM) (Hitachi, Tokyo, Japan) and a nanoparticle tracking analyzer (NTA) (Malvern, UK). According to the protocol, ADSCs were incorporated with the inhibitor of living EVs formation, namely GW4869 (20 μg/mL, Sigma–Aldrich, St. Louis, MO, USA) to obtain the conditioned medium, which was regarded as GM. EVs were preserved at −80 °C until usage.

2.5. Establishment and treatment of the animal model

In accordance with a previous report [21], the pathophysiology of OSAHS was analyzed with the application of the CIH rat model. Rats were allocated into the control group (sham), the CIH group, the CIH + GW group, and CIH + EVs group, with 12 rats per group. Rats to be treated with CIH were placed in a chamber, with the oxygen intake fraction gradually reduced to 4–5% for 15 s and then increased to 21% for 15 s with 2 min for each cycle. CIH exposure cycles were repeated 30 times per hour for 8 h per day to simulate moderate OSAHS. Rats in the sham group were raised in the chamber with normal oxygen concentration (21%). Rats in the CIH + EVs group were injected with ADSCs-EVs at a dose of 800 μg/100 μL via the caudal vein twice a week. Under the same condition, rats in the CIH + GW group were injected with the conditioned medium of the GW group [21]. The whole experimentation lasted 12 weeks.

2.6. Acquisition of tissue specimens

After anesthesia by 50 mg/kg pentobarbital sodium, rats were treated with heart puncture exsanguination. The blood samples were centrifuged at 4000 g for 10 min and preserved at −80 °C for further analyses. Next, rats were euthanatized through intraperitoneal injection of 800 mg/kg pentobarbital sodium, after which lung tissues were separated immediately. The left lung was fixed with 4% paraformaldehyde and embedded in paraffin (5 μm) for staining. The right lung was prepared into tissue homogenate for the subsequent analyses.

2.7. Histopathology and terminal-deoxynucleoitidyl transferase mediated nick end labeling (TUNEL) staining

Paraffin-embedded sections were deparaffined, dehydrated, stained with hematoxylin (Solarbio) for 3 min, washed, and differentiated in 1% acid alcohol for 15 s. Next, sections were stained with eosin (Solarbio) for 2 min. Afterwards, the lung morphology was observed under an optical microscope (Olympus). As previously described, pathologists scored lung tissue damage according to a scale of 1 (no damage) to 4 (most severe).

After de-paraffining and dehydration, apoptosis was determined using the TUNEL assay kit (Nanjing Keygen Biotech CO., Ltd., Nanjing, Jiangsu, China). Next, cell nuclei were stained with 4',6-diamidino-2-phenylindole (DAPI) (Beyotime Biotechnology Co. LTD, Shanghai, China). The TUNEL positive cells were observed by means of fluorescence microscopy (Nikon, Tokyo, Japan). The apoptosis degree was evaluated by the ratio of TUNEL positive cells within the visual field and the total cells.

2.8. Cell culture and treatment

RLE-6TN cells (ATCC, Manassas, Virginia, USA) were cultured in DMEM/F12 medium consisting of 10% FBS, 100 μg/mL streptomycin, and 100 U/mL penicillin (Sigma–Aldrich, Merck KGaA, Darmstadt, Germany). The treated cells were cultured at 37 °C with 5% CO_2 in air.

The intermittent hypoxia (IH) regimen consisted of alternative cycle of 20 min hypoxia (1% O_2 and 5% CO_2) and 20 min reoxygenation (21% O_2 and 5% CO_2), with 40 min for each cycle and a total 72 cycles and was conducted on the OxyCycler C42 system (BioSpherix, Redfield, NY, UAS). Then, RLE-6TN cells were treated with 20 μg ADSCs-EVs for 24 h before IH regimen, with GW treatment as the control [22]. In addition, RLE-6TN cells were cultured in the 6-well plates at a density of 1×10^6 cells/per well. RLE-6 TN cells were transfected with KDM6B pcDNA3.1 (oe-KDM6B) or HMGA2 pcDNA3.1 (oe-HMGA2) or the negative control (GenePharma, Shanghai, China) by means of Lipofectamine 3000. After 24 h, the transfection efficiency was tested or RLE-6TN cells were exposure to a specified number of IH cycles.

2.9. 3-(4,5-Dimethylthiazol-2-yl)-2,5-diphenyltetrazolium bromide (MTT) assay

RLE-6TN cells were cultured in the 96-well plate at a density of 2×10^3 cells/per well under the condition of 37 °C and 5% CO_2. After 48 h, each well was incorporated with 20 μL MTT solution (5 mg/mL) followed by another 4 h incubation. Subsequently, 150 mL dimethylsulfoxide was added into the well and the plate was placed in a microplate reader (Bio-Rad, Hercules, CA, USA). The absorbance at a wavelength of 492 nm was determined to evaluate cell viability.

2.10. TUNEL assay

In the TUNEL assay, RLE-6TN cells were seeded into the 6-well plate. After corresponding treatments in each group, cells were washed with PBS twice, fixed with 4% formaldehyde at 4 °C for 10 min, cleaned with PBS twice, and immersed with 3% H_2O_2 and 0.2% Triton X-100 in order for 5–10 min, followed by incubation with 100 μL equilibration buffer for 10 min at room temperature. Subsequently, RLE-6TN cells were incubated with 50 μL terminal deoxynucleoside transferase reaction cocktail at 37 °C for 60 min. Next, glass slides were washed with 2 × sodium citrate buffer for 15 min and incubated with DAPI for 15 min. Afterwards, the number of staining positive cells was determined using a fluorescence microscope.

2.11. Reactive oxygen species (ROS), malondialdehyde (MDA), superoxide dismutase (SOD), and myeloperoxidase (MPO) assays

The lung tissues were homogenized with the tissue lysis buffer (Beyotime). The tissue homogenate was lysed on ice for 15 min and treated with centrifugation (4000 g, 4 °C, 15 min). According to the protocol, MPO activity in the supernatant was determined using a MPO assay kit (A044-1-1, Nanjing Jiancheng Biological Engineering Research Institute Co., Ltd, Nanjing, China). Then, cells were lysed primarily. Cell lysate was centrifuged at 600 g and 4 °C for 10 min to collect the supernatant. According to the protocols, MDA content and SOD activity were measured using a MDA commercially available kit (A003-1-2, Nanjing Jiancheng Biological Engineering Research Institute Co., Ltd) and a SOD assay kit (A001-3-2, Nanjing Jiancheng Biological Engineering Research Institute Co., Ltd).

Following the manufacturer's instructions, ROS level was determined using a ROS assay kit (S0033S, Beyotime). For *in vivo* analysis, lung homogenate was incubated with 2′,7′-dichlorodihydrofluorescein diacetate (DCFH-DA) at 37 °C for 30 min. The change in fluorescence intensity at 500/530 nm was analyzed using a fluorescence microplate (Bio-Rad). For *in vitro* analysis, cells were incubated with DCFH-DA at 37 °C for 20 min and washed with serum-free medium. The fluorescence intensity at 488/525 nm was determined and results were shown as percentages.

2.12. Enzyme-linked immunosorbent assay (ELISA)

The levels of tumor necrosis factor (TNF)-α (ab236712), interleukin (IL)-6 (ab234570), and monocyte chemoattractant protein-1 (MCP-1) (ab219045) were measured by applying ELISA kits specific to these factors from Abcam corporation (Cambridge, MA, USA), with a microplate reader to determine the absorbance at a wavelength of 450 nm.

2.13. Co-culture of Cy3-labelled and miR-22–3p transfected ADSCs and RLE-6TN cells

ADSCs were harvested and treated with 0.25% trypsin. Then. Cy3-lablled miR-22–3p mimic (RiboBio, Guangdong, China) was transfected into ADSCs using Lipofectamin 3000. Next, ADSCs were seeded into the 6-well plates and co-cultured with RLE-6TN cells transfected with green fluorescent protein (GFP). In addition, GW4869 (10 M for 48 h) was incorporated into the above system, which was regarded as the EVs release inhibition group. Eventually, cells were observed using a confocal microscope (Leica Microsystems, Mannheim, Germany).

2.14. Dual-luciferase assay

The binding site between miR-22–3p and KDM6B 3′UTR was predicted through the online software Targetscan (http://www.targetscan.org/vert_71/) [23]. The amplified complementary binding sequence and wild-type sequence were cloned into pmiR-GLO luciferase vectors (Promega, Madison, WI, USA) to establish HDM6-wildtype (WT) and KDM6B-mutuant type (MUT) plasmids. The above plasmids were mixed with miR-22–3p mimic (mimic) or the negative control (NC). At last, the mixture was transfected into RLE-6TN cells using Lipofectamine 3000. After 48 h, the luciferase activity was determined.

2.15. Chromatin immunoprecipitation (ChIP) assay

Following the manufacturer's protocol, the ChIP assay was conducted using the EZ-ChIP assay kit (Millipore, Boston, MA, USA). In brief, RLE-6TN cells were crosslinked 1% formaldehyde, and incorporated with 125 mM glycine to terminate the reaction. Chromatins were collected and DNA was sheared by ultrasound at 4 °C, followed by overnight incubation with antibodies against H3K27me3 (MA5-11198, Thermo Fisher Scientific), KDM6B (PA5-72751, Thermo Fisher Scientific), and immunoglobulin G (ab207997, Abcam) at 4 °C. Then, chromatins were further incubated with protein G agarose for 2 h and added with 0.2 M NaCl for overnight incubation at 65 °C to reverse the crosslink of the protein-DNA compound. After that, protein was detached by proteinase K and immunoprecipitated DNA was purified. The enrichment in the HMGA2 promoter region was tested by means of real-time quantitative polymerase chain reaction (RT-qPCR). PCR primers are shown in Table 1.

Table 1
PCR primers.

Gene	Sequence (5′-3′)
miR-22–3p	F: GAGCTCAAGCTGCCAGTTGA
	R: CAACTGGTGTCGTGGAGTCG
KDM6B	F: GTACCAGGCTTCGTCCTTCC
	R: ATGGTTCTTGGGGTCTGGTG
HMGA2	F: ATGAGCGCACGCGGTGAGG
	R: GGCTCACAGGTTGGCTCTT
U6	F: ATGGCGGACGACGTAGATCA
	R: TCAGCCAACTCTCAATGGAGG
GAPDH	F: ATGGTGAAGGTCGGTGTGAAC
	R: TACTCCTTGGAGGCCATGTAG
HMGA2 promoter	F: GAACTGACCGCTTGCTTCTC
	R: TGAGGGTGGACAGGCTATGT

2.16. RT-qPCR

RNA was separated from lung tissues and RLE-6TN cells by applying the TRIzol assay kit (Invitrogen). The RNA concentration and purity were determined using an ultraviolet spectrophotometer (Thermo Fisher Scientific). RNA sample was preserved at −80 °C. Then, RNA was synthesized into the complementary DNA following the instructions of the reverse transcription assay kit (TaKaRa Biomedical Technology, Dalian, China). RT-qPCR was conducted using the SYBR Green Master Mix kit (Takara) on the CFX96 Real-Time PCR system (Bio-Rad). With GAPDH and U6 [13] serving as internal reference genes, the relative gene expression was calculated based on the $2^{-\Delta\Delta Ct}$ method [24]. Primers are shown in Table 1.

2.17. Western blot assay

The protein was separated from lung tissues and cells using radioimmunoprecipitation buffer (Sigma) containing protease inhibitor phenyl methane sulfonyl fluoride, with a bicinchoninic acid protein assay (Thermo Fisher Scientific) to determine protein concentration. An equal amount of protein was separated from loading buffer through NuPAGE 10% Bis-Tris sodium dodecyl sulfate polyacrylamide gel electrophoresis (Life Technologies, Carlsbad, CA, USA) and shifted onto polyvinylidene fluoride membranes (Millipore). The membranes were blocked with 5% bovine serum albumin for 1 h and incubated with antibodies against KDM6B (1:1000, PA5-72751, Thermo Fisher Scientific), HMGA2 (1:5000, PA5-21320, Thermo Fisher Scientific), and GAPDH (1:1000, PA1-987, Thermo Fisher Scientific) at 4 °C overnight. Following that, Western blots were washed with Tris Buffered Saline Tween three times and incubated with secondary antibody (1:5000, 31343, Thermo Fisher Scientific) at ambient temperature for 1 h. The blots were developed and exposed on Hyperfilm X-ray films using the enhanced chemiluminescence. Protein bands were quantified with the grayscale value of GAPDH as the control (Quantity-One 4.5.0 software, Bio-Rad).

2.18. Statistical analysis

All data were processed with application of SPSS21.0 statistical software (IBM SPSS Statistics, Chicago, IL, USA) and GraphPad Prism 8.0 software (GraphPad Software Inc., San Diego, CA, USA) for statistical analysis and graphing. Data testing complied to normal distribution and homogeneity of variance. Pairwise comparisons of measurement data were analyzed by the *t* test and multi-group comparisons of data were analyzed by one-way or two-way analysis of variance (ANOVA), followed by Tukey's multiple comparison test. *P* values were obtained from the two-sided test. A value of $P < 0.05$ indicated a difference with statistical significance and a

value of $P < 0.01$ indicated a difference with highly statistical significance.

3. Results

3.1. Characterization of ADSCs and ADSCs-EVs

First, we separated ADSCs and observed that most cells presented with typical pebble-like morphology (Fig. 1A). Besides, cells boasted great abilities of osteogenesis and adipogenesis differentiation (Fig. 1B–C). Surface markers of MSCs CD44 and CD105 were highly expressed but hematopoietic stem cell markers CD45 and CD34 were not expressed in cells (Fig. 1D), suggesting that the extracted cells were ADSCs. EVs from ADSCs were collected and characterized. TEM and NTA analyses revealed that the diameter of ADSCs-EVs was 120–160 nm, cup-shaped or spherical, with a particle size of about 130 nm and a concentration of 3.4×10^6 particles/mL (Fig. 1E–F). In addition, ADSCs-EVs were expressed with CD63 and CD9 but not calnexin (Fig. 1G), suggesting that ADSCs-EVs were successfully obtained.

3.2. ADSCs-EVs alleviates OSAHS-LI

We established the OSAHS rat model through CIH treatment to assess the impact of ADSCs-EVs on OSAHS-LI. As shown by Fig. 2A, inflammatory cell infiltration and pulmonary edema were evident, and lung injury score was increased in the CIH group, whereas these phenomena were alleviated in the CIH + EVs group ($P < 0.01$). As shown by Fig. 2B, apoptosis rate in the CIH group was markedly higher than that in the sham group and the apoptosis rate in the CIH + EVs group was lower in the CIH + GW group ($P < 0.01$). CIH treatment significantly upregulated the contents of TNF-α, IL-6, and MCP-1 in the serum, whereas ADSCs-EVs decreased inflammation levels ($P < 0.05$, Fig. 2C). In addition, CIH treatment elevated MPO

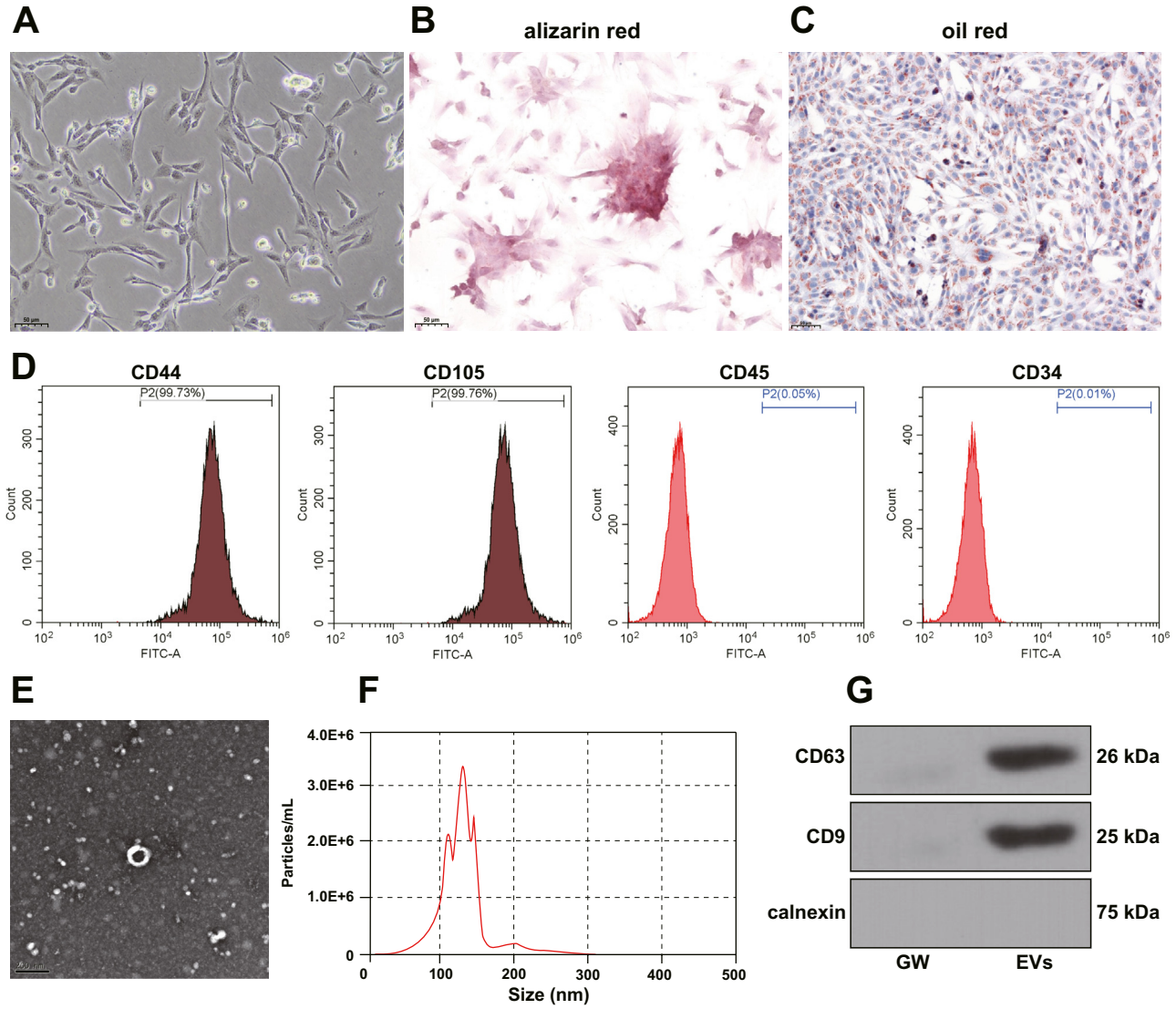

Fig. 1. ADSCs and characterization of ADSCs-EVs. A: The morphology of ADSCs was observed; B–C: Staining with alizarin red (B) and Oil red o (C) after osteogenic and adipogenic induction; D: Levels of surface CD44, CD105, CD45, and CD34 were determined by flow cytometry; E: The morphology of ADSCs-EVs was observed under a transmission electron microscope; F: Concentration and particle diameter of ADSCs-EVs were measured by a nanoparticle tracking analyzer; G: Levels of CD63, CD9, and calnexin were determined by Western blot assay. Cell experiments were repeated 3 times independently. ADSCs: adipose-derived mesenchymal stem cells; EVs: extracellular vesicles.

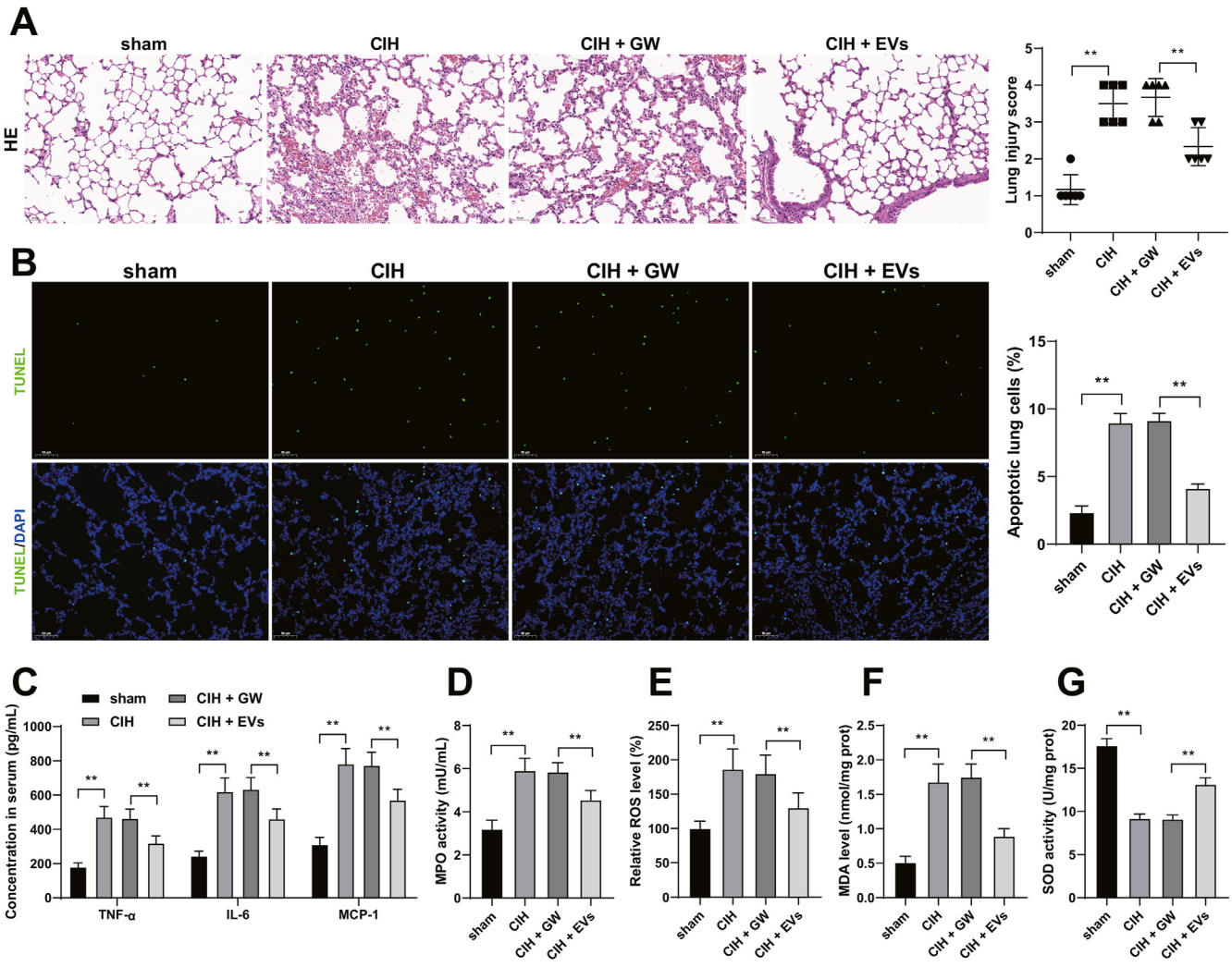

Fig. 2. ADSCs-EVs alleviates OSAHS-LI. The OSAHS rat model was established by CIH treatment and treated with ADSCs-EVs, with GW treatment as the negative control. A: The morphology of lung tissues was observed by H&E staining and lung injury scoring; B: Positive rate of TUNEL in lung tissues was determined by TUNEL staining; C: Contents of TNF-α, IL-6, and MCP-1 were determined by ELISA; D–G: MPO activity, ROS level, MDA level, and SOD activity were determined in lung tissues. N = 6. Data were shown as mean ± standard deviation. Data in panels B and D-G were analyzed by one-way ANOVA and data in panel C were analyzed by two-way ANOVA, followed by Tukey's multiple comparison test. $^{**}P < 0.01$. H&E: hematoxylin and eosin; TUNEL: terminal-deoxynucleoitidyl transferase mediated Nick end labeling; TNF-α: tumor necrosis factor; MCP-1: monocyte chemoattractant protein-1; MPO: myeloperoxidase; ROS: reactive oxygen species; MDA: malondialdehyde; SOD: superoxide dismutase.

activity, ROS levels, and MDA content and reduced SOD activity in lung tissues, while ADSCs-EVs treatment led to the opposite trends ($P < 0.05$, Fig. 2D–G). These finding suggested that ADSCs-EVs alleviated OSAHS-LI.

3.3. ADSCs-EVs alleviates IH-induced cell injury

Next, we treated RLE-6TN cells with IH and found a decrease in cell viability and an increase in apoptosis, while ADSCs-EVs treatment elevated cell viability and decreased apoptosis ($P < 0.05$, Fig. 3A–B). Relative to the control group, the contents of TNF-α, IL-6, and MCP-1 were increased, but relative to the IH + GW group, the contents of TNF-α, IL-6, and MCP-1 were diminished in the IH + EVs group ($P < 0.05$, Fig. 3C). In addition, IH induction augmented ROS levels and MDA contents and reduced SOD activity, while ADSCs-EVs reversed these results ($P < 0.05$, Fig. 3D–F). Collectively, ADSCs-EVs alleviated IH-induced pneumonocyte injury.

3.4. ADSCs-EVs delivers miR-22–3p into pneumonocytes to attenuate IH-induced cell injury

We uncovered that the expression levels of miR-22–3p were reduced in lung tissues of model rats and IH-induced pneumonocytes and were increased after ADSCs-EVs treatment ($P < 0.01$, Fig. 4A–B). Therefore, we conjectured that EVs carry miR-22–3p to play a role in OSAHS-LI. Rnase A had no impact on miR-22–3p expression, while the Rnase A combined Triton X-100 treatment obviously reduced miR-22–3p expression in conditioned culture medium ($P < 0.01$, Fig. 4C). In addition, we co-cultured Cy3-miR-22–3p mimic transfected ADSCs with GFP-transfected RLE-6TN cells and observed the presence of abundant red fluorescence in RLE-6TN cells. After the incorporation of GW4869 in the above co-culture system, there was no red fluorescence observed (Fig. 4D), suggesting that miR-22–3p was enveloped by EVs.

To verify the impact of miR-22–3p on EVs-mediated protection against OSAHS-LI, we upregulated miR-22–3p expression in ADSCs

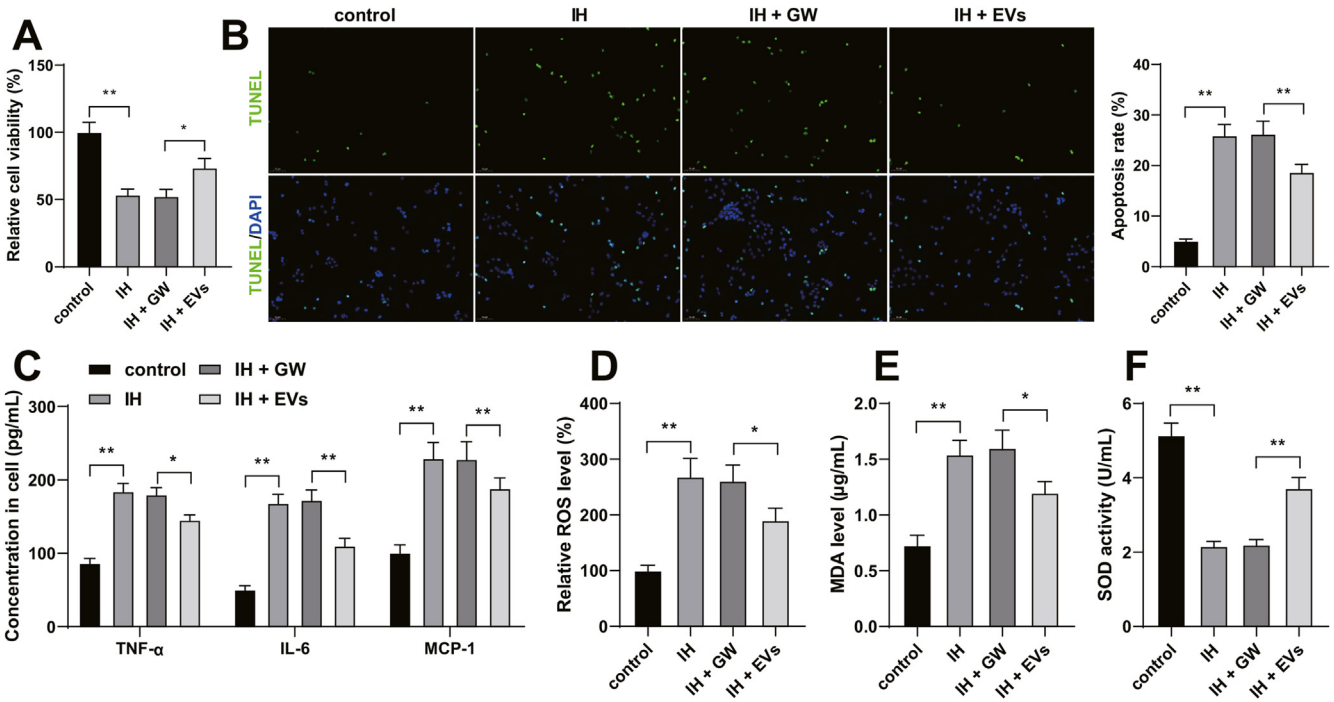

Fig. 3. ADSCs-EVs alleviates IH-induced pneumonocyte injury. IH induced RLE-6TN cell injury, followed by ADSCs-EVs treatment, with GM treatment as the negative control. A: Cell viability was assessed by MTT method; B: Apoptosis rate was assessed by TUNEL assay; C: Contents of TNF-α, IL-6, and MCP-1 were determined by ELISA; D–F: ROS and MDA levels and SOD activity in cells. The cell experiments were repeated 3 times independently. Data were shown as mean ± standard deviation. Data in panels A–B and D-F were analyzed by one-way ANOVA and data in panel C were analyzed by two-way ANOVA, followed by Tukey's multiple comparison test. *$P < 0.05$, **$P < 0.01$. IH: intermittent hypoxia; GW: GW4869 (the inhibitor of living EVs formation); MTT: 3-(4,5-dimethylthiazol-2-yl)-2,5-diphenyltetrazolium bromide; TUNEL: terminal-deoxynucleoitidyl transferase mediated Nick end labeling; TNF-α: tumor necrosis factor; MCP-1: monocyte chemoattractant protein-1; ROS: reactive oxygen species; MDA: malondialdehyde; SOD: superoxide dismutase.

followed by EVs separation, and noticed the significant elevation of miR-22−3p expression in EVs ($P < 0.05$, Fig. 4E). Subsequently, EVs-mimic was used to treat IH-induced RLE-6TN cells. It was found that EVs-mimic increased cell viability ($P < 0.05$, Fig. 4F) and decreased apoptosis ($P < 0.05$, Fig. 4G) and inflammation and oxidative stress levels ($P < 0.05$, Fig. 4I–K). Our results elicited that ADS-EVs delivered miR-22−3p into RLE-6TN cells to upregulate miR-22−3p expression and attenuate IH-induced cell injury.

3.5. miR-22−3p inhibits KDM6B and decreases HMGA2 transcription through H3K27me3

According to the binding site of miR-22−3p and KDM6B (Fig. 5A) and the results from the dual-luciferase assay, co-transfection of miR-22−3p mimic and KDM6B WT decreased luciferase activity ($P < 0.01$, Fig. 5B). Moreover, it was found that KDM6B expression levels were elevated in both *in vivo* and *in vitro* models but ADSCs-EVs treatment reduced KDM6B expression levels in lung tissues and cells and EVs-mimic treatment further decreased KDM6B expression levels ($P < 0.01$, Fig. 5C–F).

As a demethylase of H3K27me3, KDM6B can upregulate gene expression [25]. H3K27me3 modification is present on the HMGA2 promoter and HMGA2 has been shown an upregulation in lung injury [17–19]. KDM6B and H3K27me3 were enriched on the HMGA2 promoter, but EVs and EVs-mimic treatments reduced the enrichment of KDM6B and increased the enrichment of H3K27me3 ($P < 0.05$, Fig. 5G–H). In addition, the mRNA levels of HMGA2 were increased after the model establishment and decreased in response to EVs and EVs-mimic treatments ($P < 0.05$, Fig. 5I–J). Altogether, miR-22−3p targeted KDM6B and decreased its expression and further inhibited HMGA2 transcription by increasing H3K27me3 modification.

3.6. KDM6B upregulation neutralizes the protective role of ADSCs-EVs in IH-induced cell injury

Subsequently, to validate the role of KDM6B in EVs-mediated protection against OSAHS-LI, we designed the rescue experiment. First, we upregulated KDM6B expression in cells ($P < 0.01$, Fig. 6A–B), and combined with EVs to treat IH-induced cells. The results revealed that KDM6B overexpression resulted in decreased cell viability ($P < 0.05$, Fig. 6C) and increased apoptosis rate ($P < 0.05$, Fig. 6D). In addition, relative to EVs treatment alone, the combined treatment intensified both inflammation and oxidative stress ($P < 0.05$, Fig. 6E–H). The above findings suggested that KDM6B upregulation neutralized the protective role of ADSCs-EVs in IH-induced cell injury.

3.7. HMGA2 upregulation neutralizes the protective role of ADSCs-EVs in IH-induced cell injury

Eventually, we strived to testify the role of KDM6B in EVs-mediated protection against OSAHS-LI. We upregulated HMGA2 expression in cells ($P < 0.01$, Fig. 7A–B) and combined with EVs to treat IH-induced cells. Our results revealed that HMGA2 over-expression reduced cell viability and increased apoptosis ($P < 0.05$, Fig. 7C–D) and enhanced both inflammation and oxidative stress ($P < 0.05$, Fig. 7E–H). The above findings indicated that HMGA2 upregulation neutralized the protective role of ADSCs-EVs in IH-induced cell injury.

4. Discussion

Obstructive sleep apnea hypopnea syndrome (OSAHS) is an underestimated sleep disorder and is associated with CIH, which

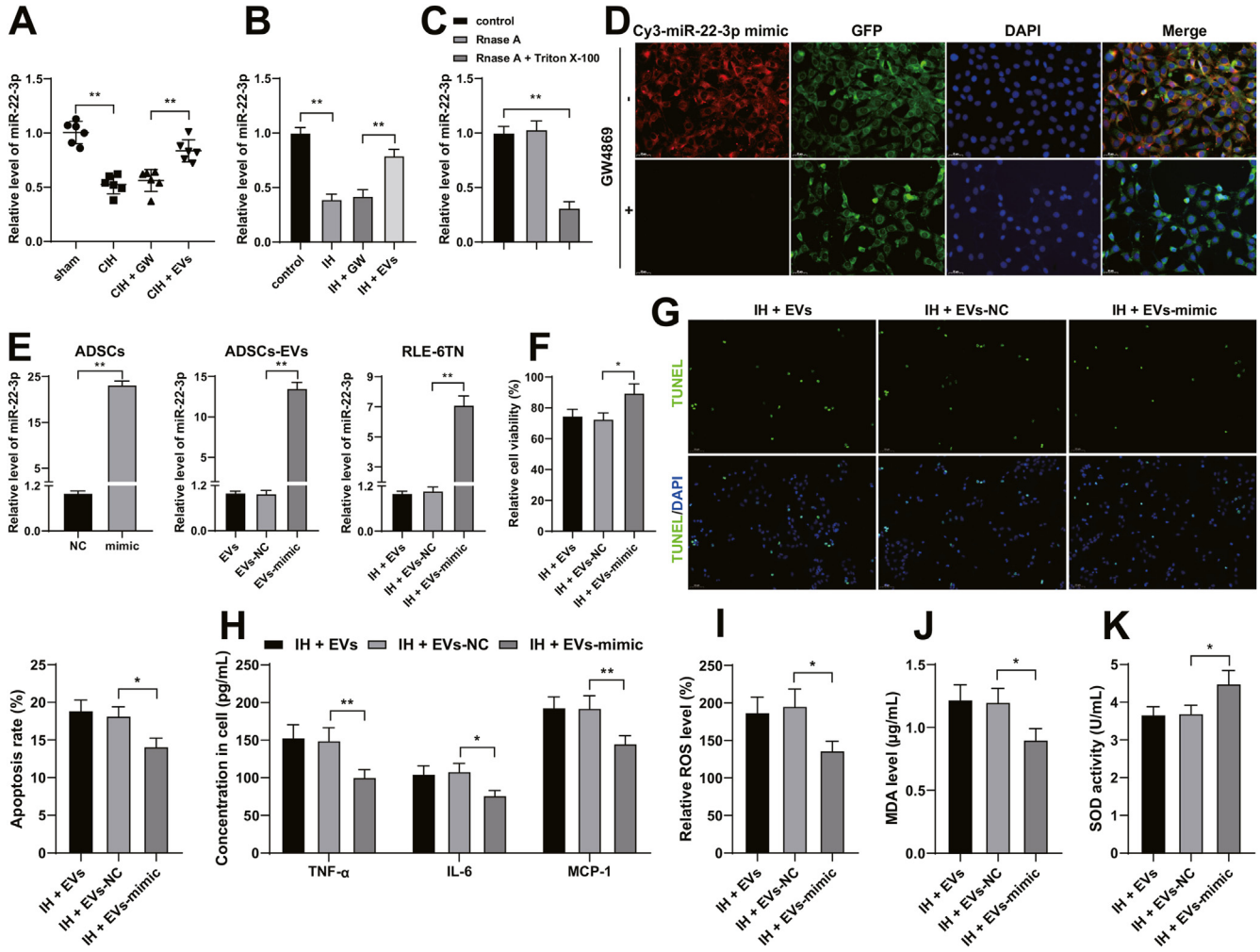

Fig. 4. ADSCs-EVs delivers miR-22−3p into pneumonocytes to attenuate IH-induced cell injury. A–B: miR-22−3p expression levels in lung tissues and cells were determined by RT-qPCR; C: miR-22−3p expression levels in ADSCs conditioned medium were determined by RT-qPCR; D: The transfer of miR-22−3p was observed by confocal microscopy; ADSCs were transfected with miR-22−3p mimic (mimic), with NC vector as the negative control, followed by separation of EVs to treat IH-induced RLE-6TN cells; E: miR-22−3p expression levels in ADSCs, ADSCs-EVs, and RLE-6TN cells were determined by RT-qPCR; F: Cell viability was assessed by the MTT method; G: Apoptosis was assessed by TUNEL assay; H: Contents of TNF-α, IL-6, and MCP-1 in cells were determined by ELISA; I–J: ROS levels, MDA levels, SOD activity in cells. N = 6, cell experiments were repeated three times independently. Data in panels B–C and E-K were shown as mean ± standard deviation. Data in panels A–C, E-G and I–K were analyzed by one-way ANOVA and data in panel H were analyzed by two-way ANOVA, followed by Tukey's multiple comparison test. $^{*}P < 0.05$, $^{**}P < 0.01$. ADSCs: adipose-derived mesenchymal stem cells; EVs: extracellular vesicles. IH: intermittent hypoxia; MTT: 3-(4,5-dimethylthiazol-2-yl)-2,5-diphenyltetrazolium bromide; TUNEL: terminal-deoxynucleoitidyl transferase mediated Nick end labeling; TNF-α: tumor necrosis factor; MCP-1: monocyte chemoattractant protein-1; ROS: reactive oxygen species; MDA: malondialdehyde; SOD: superoxide dismutase.

leads to multiple organ damages, including LI [26]. Specifically, CIH triggers the inflammation and OS cascades, which is the major cause of pneumonocyte injury [5]. Cell therapy, especially the application of MSCs, is promised to alleviate OSAHS and LI [27,28]. However, the clinical usage of MSCs is limited by the cost of culturing and preserving enough cells and their phenotype distracted by the extracellular microenvironment, while MSCs-EVs remain promising because of their ability to maintain the functional phenotype of parent cells [29]. Our study demonstrated the therapeutic function of ADSCs-EVs in OSAHS-LI by targeting the miR-22−3p/KDM6B/HMGA2 axis (Fig. 8).

ADSCs are potent to secrete plenty of cytokines, growth factors, and antioxidants to protect against inflammation and OS, thus affecting the microenvironment of their neighboring cells [30]. Besides, ADSCs are favored by the advantage of being easily and abundantly obtained by minimally invasive treatment relative to BMSCs [31]. ADSCs-EVs can improve the survival of endothelial cells to alleviate histone-induced acute lung injury [32]. Similarly, ADSCs-EVs can effectively moderate inflammation, OS, apoptosis, and necrosis in PM2.5-induced lung injury and fibrosis [33]. OS is caused by an imbalance mediated by oxidants (such as MPO) and antioxidants (such as SOD), leading to lipid peroxidation and formation of ROS and MDA [34]. ADSCs-EVs reduced apoptosis, ROS and MDA levels, and MPO activity, and increased SOD activity in CIH rats and IH-induced pneumonocytes, indicating their anti-OS property in the OSAHS-LI condition. Meanwhile, the anti-inflammatory property of ADSCs-EVs was manifested by reduced contents of inflammatory infiltration and contents of TNF-α, IL-6, and MCP-1 both *in vivo* and *in vitro*. Moreover, ADSCs-EVs after nebulization precondition not only enjoy higher clinical safety but also have higher efficacy to improve survival rate in lung injury diseases [35]. Besides, compared with exosomes from BMSCs and umbilical cord-derived MSCs, ADSCs-EVs exert a more pronounced protective role in the sepsis-induced LI mouse model [36]. Therefore, it turns out that ADSCs-EVs are a more ideal source of cell-free therapy for LI. However, regarding the scope of OSAHS, the previous

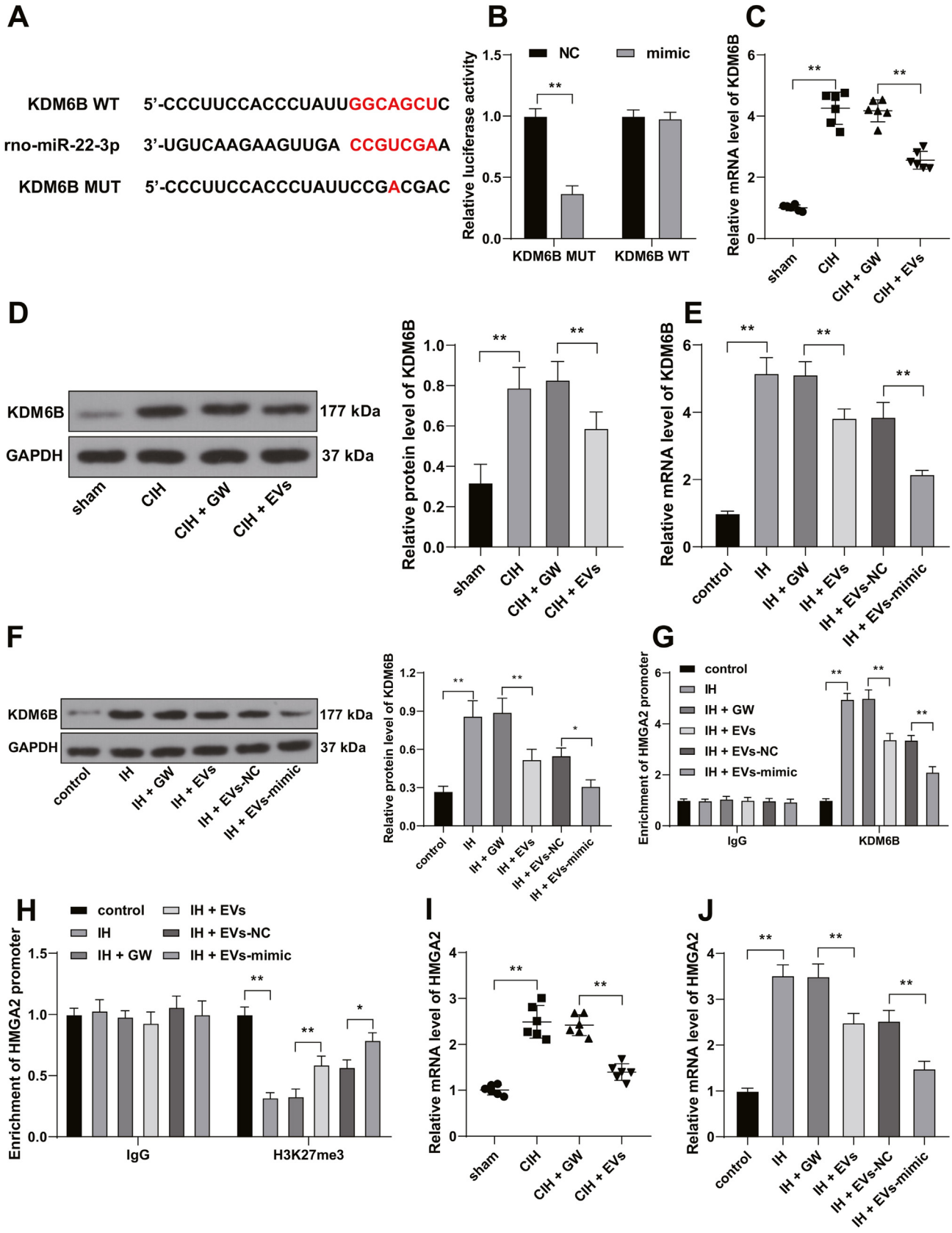

Fig. 5. miR-22−3p inhibits KDM6B and decreases HMGA2 transcription through H3K27me3. A: The binding site of miR-22−3p and KDM6B was predicted by the Targetscan database; B: The binding of miR-22−3p to KDM6B was verified by the dual-luciferase assay; C−F: KDM6B expression levels in lung tissues and cells were determined by RT-qPCR and Western blot assay; G−H: The enrichment of KDM6B or H3K27me3 on the HMGA2 promoter was measured by the ChIP assay; I−J: The mRNA levels of HMGA2 in lung tissues and cells were determined by RT-qPCR. N = 6, cell experiments were repeated 3 times independently. Data in panels B, D-H and J were shown as mean ± standard deviation. Data in panels C−F and I-J were analyzed by one-way ANOVA and data in panels B and G-H were analyzed by two-way ANOVA, followed by Tukey's multiple comparison test. *$P < 0.05$, **$P < 0.01$. ADSCs: adipose-derived mesenchymal stem cells; EVs: extracellular vesicles. IH: intermittent hypoxia; GW: GW4869 (the inhibitor of living EVs formation).

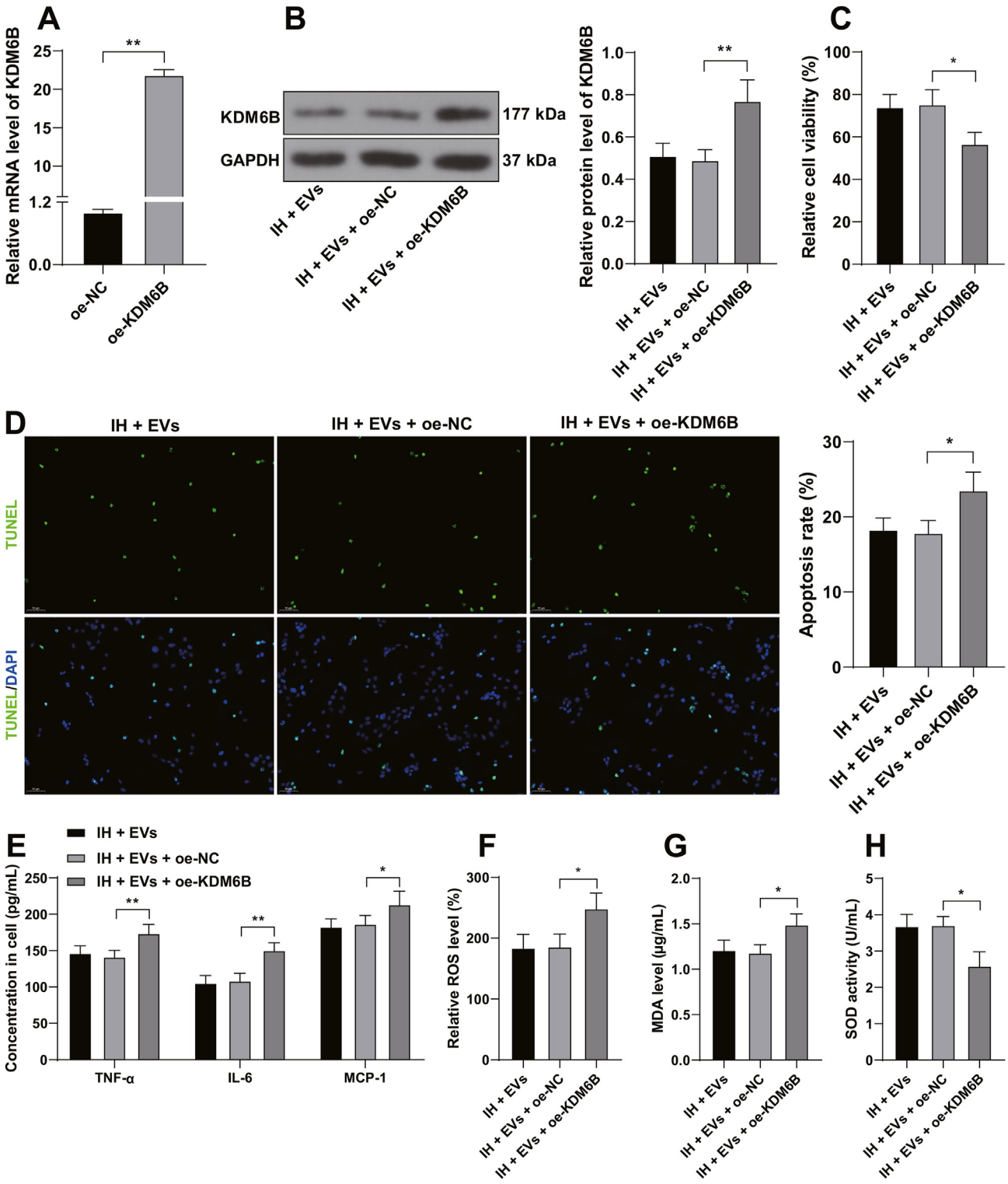

Fig. 6. KDM6B upregulation neutralizes the protective role of ADSCs-EVs in IH-induced cell injury. RLE-6 TN cells were transfected with oe-KDM6B, with oe-NC as the negative control. A–B: KDM6B expression levels in cells were determined by RT-qPCR and Western blot assay; C: Cell viability was assessed by the MTT assay; D: Cell apoptosis was assessed by the TUNEL assay; E: Contents of TNF-α, IL-6, and MCP-1 in cells were determined by ELISA; F–H: ROS levels, MDA levels, and SOD activity in cells. Cell experiments were repeated 3 times independently. Data were shown as mean ± standard deviation. Data in panel A were analyzed by the *t* test, data in panels B–D and F–H were analyzed by one-way ANOVA, and data in panel E were analyzed by two-way ANOVA, followed by Tukey's multiple comparison test. $^{*}P < 0.05$, $^{**}P < 0.01$. ADSCs: adipose-derived mesenchymal stem cells; EVs: extracellular vesicles. IH: intermittent hypoxia; MTT: 3-(4,5-dimethylthiazol-2-yl)-2,5-diphenyltetrazolium bromide; TUNEL: terminal-deoxynucleoitidyl transferase mediated Nick end labeling; TNF-α: tumor necrosis factor; MCP-1: monocyte chemoattractant protein-1; ROS: reactive oxygen species; MDA: malondialdehyde; SOD: superoxide dismutase.

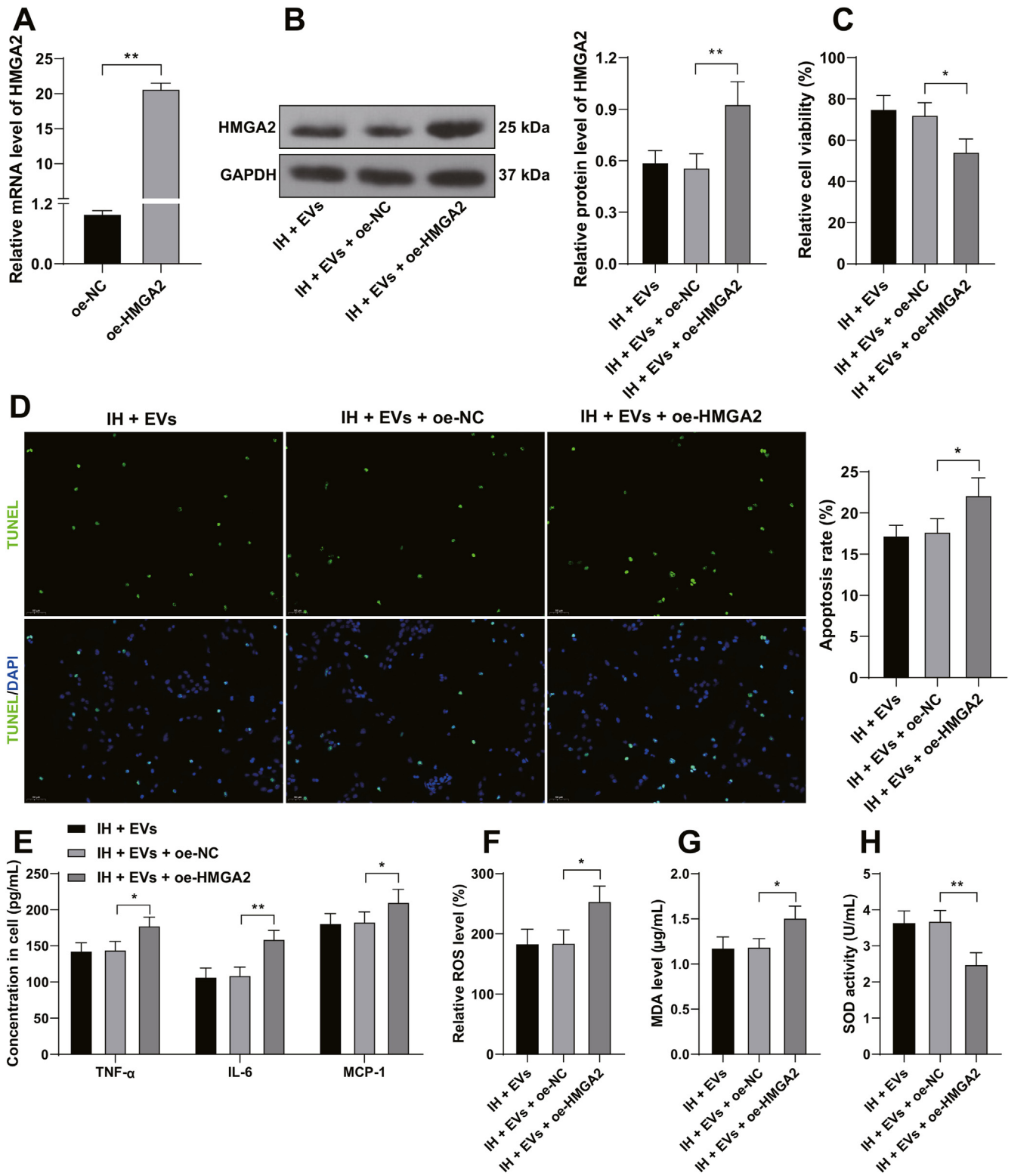

Fig. 7. HMGA2 upregulation neutralizes the protective role of ADSCs-EVs in IH-induced cell injury. RLE-6 TN cells were transfected with oe-HMGA2, with oe-NC as negative control. A–B: HMGA2 expression levels in cells were determined by RT-qPCR and Western blot assay; C: Cell viability was assessed by the MTT method; D: Apoptosis rate was assessed by TUNEL assay; E: Contents of TNF-α, IL-6, and MCP-1 in cells were determined by ELISA; F–H: ROS levels, MDA levels, and SOD activity. Cell experiments were repeated 3 times independently. Data were shown mean ± standard deviation. Data in panel A were analyzed by the *t* test, data in panels B–D and F–H were analyzed by one-way ANOVA, and data in panel E were analyzed by two-way ANOVA, followed by Tukey's multiple comparison test. $^{*}P < 0.05$, $^{**}P < 0.01$. ADSCs: adipose-derived mesenchymal stem cells; EVs: extracellular vesicles. IH: intermittent hypoxia; MTT: 3-(4,5-dimethylthiazol-2-yl)-2,5-diphenyltetrazolium bromide; TUNEL: terminal-deoxynucleoitidyl transferase mediated Nick end labeling; TNF-α: tumor necrosis factor; MCP-1: monocyte chemoattractant protein-1; ROS: reactive oxygen species; MDA: malondialdehyde; SOD: superoxide dismutase.

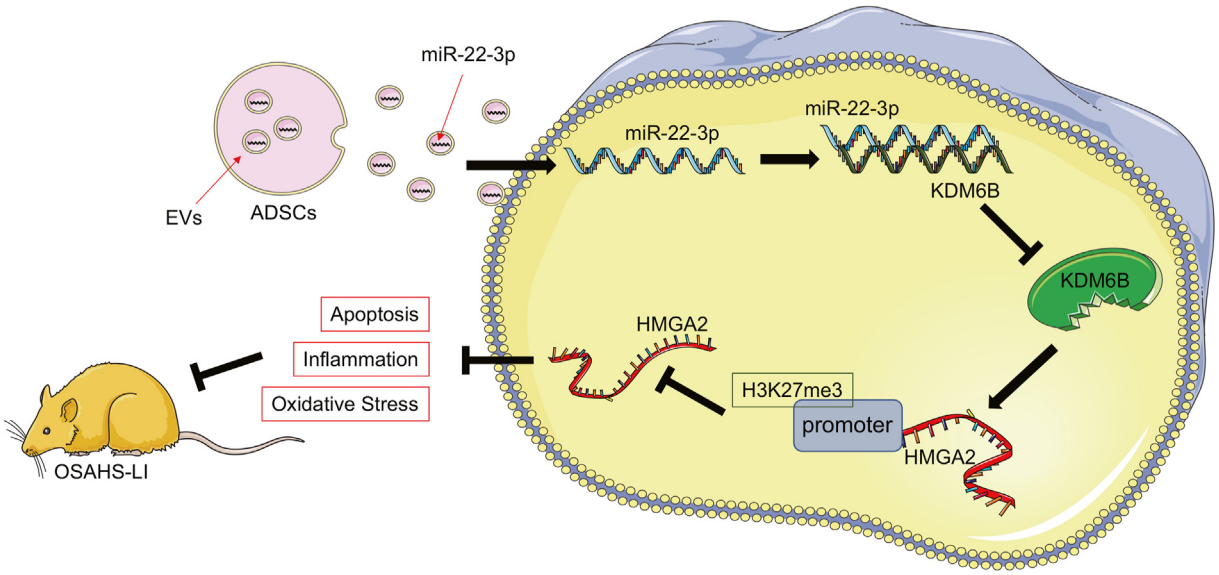

Fig. 8. Molecular mechanism of ADSCs-EV to alleviate OSAHS-LI. ADSCs-EVs delivered enveloped miR-22−3p into pneumonocytes to upregulate miR-22−3p, increased the binding of miR-22−3p to KDM6B, decreased KDM6B expression, elevated the H3K27me3 levels in the HMGA2 promoter, decreased mRNA levels of HMGA2, thus attenuating cell apoptosis, inflammation, oxidative stress, and retarding the progression of OSAHS-LI.

studies emphasized the role of BMSCs [37,38]. Our study initially substantiated the anti-OS and anti-inflammatory properties of ADSCs-EVs in OSAHS-LI, which fills the knowledge gap in OSAHS treatment.

Increasing evidence verified that ADSCs-EVs are able to mediate the transfer of miRNAs, such as miR-21−5p and miR-192 for the treatment of diseases [9,39]. Downregulated circulating miR-22−3p is associated with the pathogenesis of OSAHS [14]. miR-22−3p overexpression has been demonstrated to neutralize inflammatory and OS responses in LPS-induced acute lung injury [13]. Moreover, it is also evidenced to decrease the degree of inflammation or OS in the context of neurological disorders, sepsis-induced acute kidney injury, and hypertension [40–43]. In this study, we observed the upregulation of miR-22−3p in the lung of CIH rats and IH-induced pneumonocytes and its localization in ADSCs-EVs. Besides, the incorporation of miR-22−3p into EVs reduced apoptosis, inflammation, and OS in IH-treated cells. KDM6B is an oxygen-sensitive factor and upregulated after IH treatment [44]. Intriguingly, the aberrant expression of KDM6B is likely to trigger different modes of LI, such as acute lung injury and pulmonary ischemia/reperfusion [15,45]. Meanwhile, KDM6B can abrogate the methylation status of H3K27me3, an inhibition marker, resulting in transcriptional repression [46]. HMGA2 is a well-established oncoprotein in various cancer types [47]. Most importantly, a few studies have proved that HMGA2 promotes pulmonary fibrosis by inducing epithelial−mesenchymal transition [17,18]. Our experiments unveiled upregulated KDM6B and HMGA2 in the lung of CIH rats and IH-induced pneumonocytes. miR-22−3p negatively regulated KDM6B and KDM6B reduced the enrichment of H3K27me3 on the HMGA2 promoter to increase HMGA2 transcription. Overall, our findings elicited that ADSCs-EVs delivered miR-22−3p into pneumonocytes, which weakened the role of KDM6B in erasing H3K27me3 and then inhibited HMGA2 transcription.

Thereafter, we designed the rescue experiments to validate the roles of KDM6B and HMGA2 in OSAHS-LI. Overexpression of KDM6B and HMGA2 averted the protective role of ADSCs-EVs in CIH-induced cell injury by enhancing inflammation, apoptosis, and OS. Consistently, KDM6B is known to antagonize the anti-inflammatory signaling by modulating the methylation status [46]. For instance, KDM6B activates H3K27me3 demethylation of pro-inflammatory cytokines and enhances their transcription, thus exacerbating bacterial infection-induced inflammation [48]. In addition, activation of the HMGA2/PI3K/Akt pathway is associated with LPS-induced inflammation in corneal epithelial cells [49] and HMGA2 knockdown plays an alleviative role in high glucose-induced OS in mesangial cells [50]. Furthermore, HMGA2 is a regulator of WNT signaling in lung development [51] and WNT signaling is critical for lung healing and is altered by IH treatment [52,53]. Thus, we conjected that WNT signaling may be a downstream target of HMGA2 in ADSCs-EVs, but it requires compelling experiments to validate this conjecture. We are also aware of the limitations of our study. We only analyzed the mechanism at the cellular level, lacking validation through animal experiments and clinical analysis. miR-22−3p is only one of miRNAs that can be carried by EVs, and it is unknown whether other miRNAs from EVs exert function in the disease. Since the CIH model only simulates OSAHS-LI, our findings require more validation before applying to the clinic setting. Finally, as a transcription factor, the downstream mechanism of HMGA2 remains a mystery. Therefore, future studies are required to validate our mechanism through animal experiments and explore more miRNAs and the downstream mechanism of HMGA2, providing updated theoretical knowledge for the treatment of OSAHS-LI.

In summary, ADSCs-EVs delivered miR-22−3p into pneumonocytes to inhibit KDM6B expression, upregulate H3K27me3 level, and reduce HMGA2 transcription, thus alleviating apoptosis, inflammation, and OS and retarding the progression of OSAHS-LI. Our findings may provide novel insights into the cell-free therapy for OSAHS-LI.

Funding

None.

Ethics statement

All animal experiments were conducted following the guidelines ratified by the Ethics Committee of Guizhou Provincial People's Hospital.

Declaration of competing interest

The authors have no conflicts of interest to declare.

Acknowledgements

Not applicable.

References

[1] Iannella G, Magliulo G, Greco A, de Vincentiis M, Ralli M, Maniaci A, et al. Obstructive sleep apnea syndrome: from symptoms to treatment. Int J Environ Res Publ Health 2022;19(4):2459.
[2] Lee JJ, Sundar KM. Evaluation and management of adults with obstructive sleep apnea syndrome. Lung 2021;199(2):87–101.
[3] Zhang H, Yang F, Guo Y, Wang L, Fang F, Wu H, et al. The contribution of chronic intermittent hypoxia to OSAHS: from the perspective of serum extracellular microvesicle proteins. Metabolism 2018;85:97–108.
[4] Bostanci A, Bozkurt S, Turhan M. Impact of age on intermittent hypoxia in obstructive sleep apnea: a propensity-matched analysis. Sleep Breath 2018;22(2):317–22.
[5] Kim SW, Kim IK, Yeo CD, Kang HH, Ban WH, Kwon HY, et al. Effects of chronic intermittent hypoxia caused by obstructive sleep apnea on lipopolysaccharide-induced acute lung injury. Exp Lung Res 2020;46(9):341–51.
[6] Samsonraj RM, Raghunath M, Nurcombe V, Hui JH, van Wijnen AJ, Cool SM. Concise review: multifaceted characterization of human mesenchymal stem cells for use in regenerative medicine. Stem Cells Transl Med 2017;6(12):2173–85.
[7] Fang Y, Zhang Y, Zhou J, Cao K. Adipose-derived mesenchymal stem cell exosomes: a novel pathway for tissues repair. Cell Tissue Bank 2019;20(2):153–61.
[8] Bunnell BA. Adipose tissue-derived mesenchymal stem cells. Cells 2021;10(12):3433.
[9] Wu Y, Zhang Z, Li J, Zhong H, Yuan R, Deng Z, et al. Mechanism of adipose-derived mesenchymal stem cell-derived extracellular vesicles carrying miR-21-5p in hyperoxia-induced lung injury. Stem Cell Rev Rep 2022;18(3):1007–24.
[10] Groot M, Lee H. Sorting mechanisms for MicroRNAs into extracellular vesicles and their associated diseases. Cells 2020;9(4):1044.
[11] Boateng E, Krauss-Etschmann S. miRNAs in lung development and diseases. Int J Mol Sci 2020;21(8):2765.
[12] Correia de Sousa M, Gjorgjieva M, Dolicka D, Sobolewski C, Foti M. Deciphering miRNAs' action through miRNA editing. Int J Mol Sci 2019;20(24):6249.
[13] Zheng Y, Liu J, Chen P, Lin L, Luo Y, Ma X, et al. Exosomal miR-22-3p from human umbilical cord blood-derived mesenchymal stem cells protects against lipopolysaccharid-induced acute lung injury. Life Sci 2021;269:119004.
[14] Shao H, Shen P, Chen J. Expression profile analysis and image observation of miRNA in serum of patients with obstructive sleep apnea-hypopnea syndrome. Contrast Media Mol Imaging 2021;2021:9731502.
[15] Hong H, Huang Q, Cai Y, Lin T, Xia F, Jin Z. Dexmedetomidine preconditioning ameliorates lung injury induced by pulmonary ischemia/reperfusion by upregulating promoter histone H3K4me3 modification of KGF-2. Exp Cell Res 2021;406(2):112762.
[16] Montibus B, Cercy J, Bouschet T, Charras A, Maupetit-Mehouas S, Nury D, et al. TET3 controls the expression of the H3K27me3 demethylase Kdm6b during neural commitment. Cell Mol Life Sci 2021;78(2):757–68.
[17] Wang YC, Liu JS, Tang HK, Nie J, Zhu JX, Wen LL, et al. miR-221 targets HMGA2 to inhibit bleomycin-induced pulmonary fibrosis by regulating TGF-beta1/Smad3-induced EMT. Int J Mol Med 2016;38(4):1208–16.
[18] Liang H, Gu Y, Li T, Zhang Y, Huangfu L, Hu M, et al. Integrated analyses identify the involvement of microRNA-26a in epithelial-mesenchymal transition during idiopathic pulmonary fibrosis. Cell Death Dis 2014;5(5):e1238.
[19] Deng X, Kong F, Li S, Jiang H, Dong L, Xu X, et al. A KLF4/PiHL/EZH2/HMGA2 regulatory axis and its function in promoting oxaliplatin-resistance of colorectal cancer. Cell Death Dis 2021;12(5):485.
[20] Pan J, Alimujiang M, Chen Q, Shi H, Luo X. Exosomes derived from miR-146a-modified adipose-derived stem cells attenuate acute myocardial infarction-induced myocardial damage via downregulation of early growth response factor 1. J Cell Biochem 2019;120(3):4433–43.
[21] Ding W, Zhang X, Zhang Q, Dong Y, Wang W, Ding N. Adiponectin ameliorates lung injury induced by intermittent hypoxia through inhibition of ROS-associated pulmonary cell apoptosis. Sleep Breath 2021;25(1):459–70.
[22] Zhou Q, Zhang MM, Liu M, Tan ZG, Qin QL, Jiang YG. LncRNA XIST sponges miR-199a-3p to modulate the Sp1/LRRK2 signal pathway to accelerate Parkinson's disease progression. Aging (Albany NY) 2021;13(3):4115–37.
[23] Agarwal V, Bell GW, Nam JW, Bartel DP. Predicting effective microRNA target sites in mammalian mRNAs. Elife 2015;4:e05005.
[24] Livak KJ, Schmittgen TD. Analysis of relative gene expression data using real-time quantitative PCR and the 2(-Delta Delta C(T)) Method. Methods 2001;25(4):402–8.
[25] He Z, Wang H, Yue L. Endothelial progenitor cells-secreted extracellular vesicles containing microRNA-93-5p confer protection against sepsis-induced acute kidney injury via the KDM6B/H3K27me3/TNF-alpha axis. Exp Cell Res 2020;395(2):112173.
[26] Hou Y, Xu N, Li S, Zhang N, Ren W, Hua Z, et al. Mechanism of SMND-309 against lung injury induced by chronic intermittent hypoxia. Int Immunopharm 2022;105:108576.
[27] Xiao K, He W, Guan W, Hou F, Yan P, Xu J, et al. Mesenchymal stem cells reverse EMT process through blocking the activation of NF-kappaB and Hedgehog pathways in LPS-induced acute lung injury. Cell Death Dis 2020;11(10):863.
[28] Carreras A, Almendros I, Montserrat JM, Navajas D, Farre R. Mesenchymal stem cells reduce inflammation in a rat model of obstructive sleep apnea. Respir Physiol Neurobiol 2010;172(3):210–2.
[29] Liu A, Zhang X, He H, Zhou L, Naito Y, Sugita S, et al. Therapeutic potential of mesenchymal stem/stromal cell-derived secretome and vesicles for lung injury and disease. Expet Opin Biol Ther 2020;20(2):125–40.
[30] Rochette L, Mazini L, Malka G, Zeller M, Cottin Y, Vergely C. The crosstalk of adipose-derived stem cells (ADSC), oxidative stress, and inflammation in protective and adaptive responses. Int J Mol Sci 2020;21(23):9262.
[31] Lee RH, Kim B, Choi I, Kim H, Choi HS, Suh K, et al. Characterization and expression analysis of mesenchymal stem cells from human bone marrow and adipose tissue. Cell Physiol Biochem 2004;14(4–6):311–24.
[32] Mizuta Y, Akahoshi T, Guo J, Zhang S, Narahara S, Kawano T, et al. Exosomes from adipose tissue-derived mesenchymal stem cells ameliorate histone-induced acute lung injury by activating the PI3K/Akt pathway in endothelial cells. Stem Cell Res Ther 2020;11(1):508.
[33] Gao Y, Sun J, Dong C, Zhao M, Hu Y, Jin F. Extracellular vesicles derived from adipose mesenchymal stem cells alleviate pm2.5-induced lung injury and pulmonary fibrosis. Med Sci Mon Int Med J Exp Clin Res 2020;26:e922782.
[34] Khosravi M, Poursaleh A, Ghasempour G, Farhad S, Najafi M. The effects of oxidative stress on the development of atherosclerosis. Biol Chem 2019;400(6):711–32.
[35] Shi MM, Yang QY, Monsel A, Yan JY, Dai CX, Zhao JY, et al. Preclinical efficacy and clinical safety of clinical-grade nebulized allogenic adipose mesenchymal stromal cells-derived extracellular vesicles. J Extracell Vesicles 2021;10(10):e12134.
[36] Deng H, Zhu L, Zhang Y, Zheng L, Hu S, Zhou W, et al. Differential lung protective capacity of exosomes derived from human adipose tissue, bone marrow, and umbilical cord mesenchymal stem cells in sepsis-induced acute lung injury. Oxid Med Cell Longev 2022;2022:7837837.
[37] Bi H, He J, He X, Du J, Chen M, Huang Z, et al. Bone marrow stem cells therapy alleviates vascular injury in a chronic obstructive pulmonary disease-obstructive sleep apnea overlap syndrome rat model. Mol Med Rep 2021;23(1). Article Number:69.
[38] Chen M, Huang Z, Bi H, Pan X, He J, He L, et al. Effects of bone marrow-derived mesenchymal stem cell transplantation on chronic obstructive pulmonary disease/obstructive sleep apnea overlap syndrome in rats. Mol Med Rep 2019;20(5):4665–73.
[39] Gu C, Zhang H, Gao Y. Adipose mesenchymal stem cells-secreted extracellular vesicles containing microRNA-192 delays diabetic retinopathy by targeting ITGA1. J Cell Physiol 2021;236(7):5036–51.
[40] Chen H, Xu X, Liu Z, Wu Y. MiR-22-3p suppresses vascular remodeling and oxidative stress by targeting CHD9 during the development of hypertension. J Vasc Res 2021;58(3):180–90.
[41] Ge QM, Huang CM, Zhu XY, Bian F, Pan SM. Differentially expressed miRNAs in sepsis-induced acute kidney injury target oxidative stress and mitochondrial dysfunction pathways. PLoS One 2017;12(3):e0173292.
[42] Ren Y, Sun-Waterhouse D, Ouyang F, Tan X, Li D, Xu L, et al. Apple phenolic extracts ameliorate lead-induced cognitive impairment and depression- and anxiety-like behavior in mice by abating oxidative stress, inflammation and apoptosis via the miR-22-3p/SIRT1 axis. Food Funct 2022;13(5):2647–61.
[43] Wang X, Wang Y, Kong M, Yang J. MiR-22-3p suppresses sepsis-induced acute kidney injury by targeting PTEN. Biosci Rep 2020;40(6):BSR20200527.
[44] Nanduri J, Wang N, Wang BL, Prabhakar NR. Lysine demethylase KDM6B regulates HIF-1alpha-mediated systemic and cellular responses to intermittent hypoxia. Physiol Genom 2021;53(9):385–94.
[45] Peng J, Fan B, Bao C, Jing C. JMJD3 deficiency alleviates lipopolysaccharide-induced acute lung injury by inhibiting alveolar epithelial ferroptosis in a Nrf2-dependent manner. Mol Med Rep 2021;24(5). Article Number:807.
[46] Nakka K, Hachmer S, Mokhtari Z, Kovac R, Bandukwala H, Bernard C, et al. JMJD3 activated hyaluronan synthesis drives muscle regeneration in an inflammatory environment. Science 2022;377(6606):666–9.
[47] Mansoori B, Mohammadi A, Ditzel HJ, Duijf PHG, Khaze V, Gjerstorff MF, et al. HMGA2 as a critical regulator in cancer development. Genes 2021;12(2):269.
[48] Wu C, Chen W, He J, Jin S, Liu Y, Yi Y, et al. Interplay of m(6)A and H3K27 trimethylation restrains inflammation during bacterial infection. Sci Adv 2020;6(34):eaba0647.

[49] Li X, Sun M, Long Y. Cyanidin-3-O-Glucoside attenuates lipopolysaccharide-induced inflammation in human corneal epithelial cells by inducing let-7b-5p-mediated HMGA2/PI3K/akt pathway. Inflammation 2020;43(3):1088–96.
[50] Li J, Li M, Bai L. KCNQ1OT1/miR-18b/HMGA2 axis regulates high glucose-induced proliferation, oxidative stress, and extracellular matrix accumulation in mesangial cells. Mol Cell Biochem 2021;476(1):321–31.
[51] Singhl,MehtaA,ContrerasA,BoettgerT,CarraroG,WheelerM,etal.Hmga2isrequired for canonical WNT signaling during lung development. BMC Biol 2014;12:21.
[52] Wu J, Stefaniak J, Hafner C, Schramel JP, Kaun C, Wojta J, et al. Intermittent hypoxia causes inflammation and injury to human adult cardiac myocytes. Anesth Analg 2016;122(2):373–80.
[53] Villar J, Zhang H, Slutsky AS. Lung repair and regeneration in ARDS: role of PECAM1 and wnt signaling. Chest 2019;155(3):587–94.